
Fidelity-susceptibility analysis of the honeycomb-lattice Ising antiferromagnet under the imaginary magnetic field

Yoshihiro Nishiyama

Received: date / Accepted: date

Abstract The honeycomb-lattice Ising antiferromagnet subjected to the imaginary magnetic field $H = i\theta T/2$ with the “topological” angle θ and temperature T was investigated numerically. In order to treat such a complex-valued statistical weight, we employed the transfer-matrix method. As a probe to detect the order-disorder phase transition, we resort to an extended version of the fidelity F , which makes sense even for such a non-hermitian transfer matrix. As a preliminary survey, for an intermediate value of θ , we investigated the phase transition via the fidelity susceptibility $\chi_F^{(\theta)}$. The fidelity susceptibility $\chi_F^{(\theta)}$ exhibits a notable signature for the criticality as compared to the ordinary quantifiers such as the magnetic susceptibility. Thereby, we analyze the endpoint singularity of the order-disorder phase boundary at $\theta = \pi$. We cast the $\chi_F^{(\theta)}$ data into the crossover-scaling formula with $\delta\theta = \pi - \theta$ scaled carefully. Our result for the crossover exponent ϕ seems to differ from the mean-field and square-lattice values, suggesting that the lattice structure renders subtle influences as to the multi-criticality at $\theta = \pi$.

1 Introduction

The concept of fidelity has been developed in the field of the quantum dynamics [1,2,3,4]. The fidelity F is given by the overlap $F = |\langle\theta|\theta + \Delta\theta\rangle|$ between the ground states, $|\theta\rangle$ and $|\theta + \Delta\theta\rangle$, with the proximate interaction parameters, θ and $\theta + \Delta\theta$, respectively; see Refs. [5,6,7] for a review. Meanwhile, it turned out that it detects the quantum phase transitions rather sensitively [8,9,10,11,12,13,14]. Actually, the fidelity susceptibility $\chi_F = -\frac{1}{N}\partial_{\Delta\theta}^2 F|_{\Delta\theta=0}$ (N : number of lattice points) exhibits a pronounced signature for the criticality as compared to the ordinary quantifiers such as the magnetic susceptibility [15]. Additionally, the fidelity susceptibility does not rely on any presumptions

Department of Physics, Faculty of Science, Okayama University, Okayama 700-8530, Japan

as to the order parameter concerned [16], and it is less influenced by the finite-size artifacts [11]. As would be apparent from the definition, the fidelity $F = |\langle \theta | \theta + \Delta \theta \rangle|$ fits the numerical diagonalization method, which admits the ground-state vector $|\theta\rangle$ explicitly. However, It has to be mentioned that the fidelity is accessible via the quantum Monte Carlo method [15, 16, 17, 18] and the experimental observations [19, 20, 21] as well.

In this paper, by the agency of the fidelity, we investigate the honeycomb-lattice Ising antiferromagnet under the imaginary magnetic field. To cope with the complex-valued statistical weight, we employed the transfer-matrix method [22, 23] through resorting to the extended version of the fidelity [17, 24]

$$F = \sqrt{\frac{[\mathbf{v}_L(\theta + \Delta\theta) \cdot \mathbf{v}_R(\theta)][\mathbf{v}_L(\theta) \cdot \mathbf{v}_R(\theta + \Delta\theta)]}{[\mathbf{v}_L(\theta) \cdot \mathbf{v}_R(\theta)][\mathbf{v}_L(\theta + \Delta\theta) \cdot \mathbf{v}_R(\theta + \Delta\theta)]}}, \quad (1)$$

which makes sense even for such a non-hermitian transfer matrix. Here, the right and left eigenvectors $\mathbf{v}_R(\theta)$ and $\mathbf{v}_L(\theta)$ satisfy

$$T(\theta)\mathbf{v}_R(\theta) = \lambda_1\mathbf{v}_R(\theta) \quad (2)$$

and

$${}^t\mathbf{v}_L(\theta)T(\theta) = \lambda_1{}^t\mathbf{v}_L(\theta), \quad (3)$$

respectively, with the maximal eigenvalue λ_1 of the transfer matrix $T(\theta)$. Notably, the expression (1) reduces to the aforementioned one $|\langle \theta | \theta + \Delta \theta \rangle|$, provided that the matrix $T(\theta)$ is hermitian, and the vectors $\mathbf{v}_{R,L}$ are adjoint. In the present work, the matrix $T(\theta)$ is non-symmetric and complex-valued, and it is by no means hermitian. So far, the real-non-symmetric [24] and complex-valued-symmetric [22, 25] transfer matrices were treated for the quantum XXZ chain and square-lattice Ising antiferromagnet under the imaginary field, respectively. In this paper, we demonstrate that the complex-valued non-symmetric T , namely, the honeycomb-lattice case, is also tractable with the simulation scheme. It is anticipated that the criticality of the honeycomb-lattice model is not identical to that of the square-lattice model, because the former possesses the duality [26, 27, 28] at a finely-tuned value of the imaginary magnetic field.

To be specific, we present the Hamiltonian for the honeycomb-lattice Ising antiferromagnet subjected to the imaginary magnetic field

$$\mathcal{H} = J \sum_{\langle ij \rangle} S_i S_j - H \sum_i S_i. \quad (4)$$

Here, the Ising spin $S_i = \pm 1$ is placed at each honeycomb-lattice point $i = 1, 2, \dots, N$, and the summation $\sum_{\langle ij \rangle}$ runs over all possible nearest-neighbor pairs $\langle ij \rangle$. Hereafter, the antiferromagnetic coupling constant J is regarded as the unit of energy $J = 1$. The magnetic field H takes a pure imaginary value

$$H = i\theta T/2, \quad (5)$$

with the ‘‘topological’’ angle θ , and temperature T , and likewise, the reduced coupling constant $K = J/T$ is introduced.

A schematic drawing of the phase diagram [26,27,28,29,30,31] is presented in Fig. 1 (a). The order-disorder phase boundary extends into the finite- θ regime, and eventually, the phase boundary terminates at $\theta = \pi$. So far, the model (4) has been investigated by means of the partition-function zeros [29], albeit with an emphasis on the *real-H*-driven criticality. Additionally, rigorous information in terms of the duality theory [26,27,28,30,31] is available at $\theta = \pi$. In fairness, it has to be mentioned that the *square*-lattice counterpart has been investigated with the partition-function-zeros [32], series-expansion [33], and exact-diagonalization [25] methods in order to surmount the severe sign problem due to the imaginary magnetic field [34]. In particular, the series expansion has played a significant role; actually, the above-mentioned works, Ref. [30] and [33], made use of the low-temperature and cumulant expansions, respectively, elucidating the underlying criticality rather systematically. The phase diagram, Fig. 1 (a), should resemble that of the square-lattice model in overall characters. In contrast, the ferromagnetic counterpart does exhibit no phase transition in the finite- θ domain according to the celebrated theory of the Lee-Yang zeros [35].

Then, there arises a problem how the phase boundary ends up at $\theta = \pi$; see Fig. 1 (b). The mean-field result [34] shows that the phase boundary is curved convexly around $\theta \approx \pi$, characterized [36,37] by the crossover exponent $\phi(= 1/2) < 1$. On the contrary, the above mentioned numerical results [32, 33,25] for the square-lattice model indicate a concavely-curved phase boundary with $\phi > 1$. Because the honeycomb-lattice antiferromagnet at $\theta = \pi$ is under the reign of the duality theory [26,27,28,30], the end-point singularity ϕ should reflect its peculiar characters. The aim of this paper is to explore ϕ quantitatively by casting the fidelity-susceptibility data into the crossover-scaling theory [36,37]; a key ingredient is that the probe $\chi_F^{(\theta)}$ exhibits a notable singularity at the end-point $\theta = \pi$.

The rest of this paper is organized as follows. In Sec. 2, we present the numerical results. The transfer-matrix scheme is outlined as well. In Sec. 3, we address the summary and discussions.

2 Numerical results

In this section, we present the numerical results for the honeycomb-lattice Ising antiferromagnet under the imaginary magnetic field (4). In order to cope with the complex-valued statistical weight, we employed the transfer-matrix method as developed in Ref. [22], where the authors investigated the *square*-lattice version rather in detail; our simulation scheme owes to this development. In Fig. 2, we present a unit of the transfer-matrix slice for the honeycomb-lattice model. The row-to-row statistical weight between the spin arrangements, S_i and T_i ($i = 1, 2, \dots, L$), yields the transfer-matrix element, $T_{\{S_i\},\{T_i\}}$. Here, we implemented the periodic-boundary condition such as $S_{L+1} = S_1$ and

$T_{L+1} = T_1$. As would be apparent from Fig. 2, the transfer matrix is not symmetric, $T_{\{S_i\},\{T_i\}} \neq T_{\{T_i\},\{S_i\}}$, in contrast to that of the square-lattice case [22]. Correspondingly, in the present case, the left and right eigenvectors, \mathbf{v}_L and \mathbf{v}_R , are neither identical nor adjoint, and the extension of the fidelity (1) now becomes essential.

Provided that the fidelity F (1) is at hand, we are able to evaluate the fidelity susceptibility

$$\chi_F^{(\theta)} = -\frac{1}{L} \partial_{\Delta\theta}^2 F|_{\Delta\theta=0}. \quad (6)$$

According to the scaling theory [15], the fidelity susceptibility (6) exhibits an enhanced singularity as compared to the ordinary quantifiers such as the magnetic susceptibility. Note that for the two-dimensional Ising antiferromagnet, both specific heat and *uniform* susceptibility exhibit weak (logarithmic) singularities at the Néel temperature. Hence, it is significant to search for alternative quantifiers so as to detect the signature for the criticality.

2.1 Finite-size-scaling analysis of the fidelity susceptibility $\chi_F^{(\theta)}$ (6) with the fixed $\theta = 2.22$

In this section, via the fidelity susceptibility $\chi_F^{(\theta)}$ (6), we investigate the order-disorder phase transition of the honeycomb-lattice antiferromagnet with an intermediate value of the imaginary magnetic field $\theta = 2.22$. At this point $\theta = 2.22$, a preceding simulation result [29] is available.

In Fig. 3, we present the approximate critical point $K_c(L)$ for $1/L$ with the fixed $\theta = 2.22$ and various system sizes $L = 14, 16, \dots, 20$. Here, the approximate critical point $K_c(L)$ denotes the maximal point of the fidelity susceptibility

$$\partial_K \chi_F^{(\theta)}|_{K=K_c(L)} = 0, \quad (7)$$

for each L . The least-squares fit to these data yields an estimate $K_c = 0.48392(55)$ in the thermodynamic limit $L \rightarrow \infty$. As a reference, we carried out the similar extrapolation scheme with the abscissa scale replaced with $1/L^2$, and we arrived at an alternative estimate $K_c = 0.47969(12)$. The deviation between them ≈ 0.004 dominates the least-squares-fitting error ≈ 0.00055 . Hence, regarding the former 0.004 as a possible systematic error, we estimate the critical point as

$$K_c = 0.484(4). \quad (8)$$

The estimate (8) is to be compared with the preceding result $K_c|_{\theta=2.22} = 0.458\dots$ [29]; see Table 1. In Ref. [29], the distribution of the partition-function zeros was explored for the honeycomb-lattice antiferromagnet, albeit with an emphasis on the *real-H*-driven phase transition; afterward, we explain how the transition point was extracted from their simulation result. As presented in Table 1, our result $K_c|_{\theta=2.22} = 0.484(4)$ [Eq. (8)] is comparable to this elaborated pioneering study, $K_c|_{\theta=2.22} = 0.458$ [29]. Such a feature validates the

use of the $\chi_F^{(\theta)}$ -mediated simulation scheme even for the case of non-symmetric complex-valued transfer matrix of the honeycomb-lattice model (4).

We then turn to the analysis of the criticality, namely, $\chi_F^{(\theta)}$'s scaling dimension $\alpha_F^{(\theta)}/\nu$ [15]. Here, the index $\alpha_F^{(\theta)}$ (ν) denotes the fidelity-susceptibility (correlation-length) critical exponent such as $\chi_F^{(\theta)} \sim |K - K_c|^{-\alpha_F^{(\theta)}}$ ($\xi \sim |K - K_c|^{-\nu}$). In Fig. 4, the approximate critical exponent $\alpha_F^{(\theta)}/\nu(L, L + 2)$ is plotted for $1/(L + 1)^2$ with the fixed $\theta = 2.22$ and various system sizes $L = 14, 16, 18$. Here, the approximate critical exponent is given by the logarithmic derivative of $\ln \chi_F^{(\theta)}(L)$

$$\frac{\alpha_F^{(\theta)}}{\nu}(L, L') = \frac{\ln(\chi_F^{(\theta)}(L)|_{K_c(L)}/\chi_F^{(\theta)}(L')|_{K_c(L')})}{\ln(L/L')}, \quad (9)$$

for a pair of system sizes (L, L') . The least-squares fit to these data yields an estimate $\alpha_F^{(\theta)}/\nu = 0.9652(22)$ in the thermodynamic limit $L \rightarrow \infty$. Alternatively, we arrive at $\alpha_F^{(\theta)}/\nu = 0.9986(38)$ with the abscissa scale replaced with $1/(L + 1)^3$. The deviation between them ≈ 0.03 dominates the least-squares-fitting error ≈ 0.0022 . Hence, considering the former as a possible systematic error, we estimate the critical exponent as

$$\alpha_F^{(\theta)}/\nu = 0.97(3). \quad (10)$$

According to the scaling theory [15], the scaling relation

$$\alpha_F^{(\theta)}/\nu = \gamma_{af}/\nu + 1, \quad (11)$$

holds with the magnetic-susceptibility critical exponent for the antiferromagnet γ_{af} . Putting our result $\alpha_F^{(\theta)}/\nu = 0.97(3)$ [Eq. (10)] into this scaling relation (11), we obtain

$$\gamma_{af}/\nu = -0.03(3). \quad (12)$$

This result indicates that the phase transition belongs to the two-dimensional-Ising universality class, $\gamma_{af} = 0$ (logarithmic) [38, 39].

A few remarks are in order. First, we stress that $\chi_F^{(\theta)}$'s scaling dimension, $\alpha_F^{(\theta)}/\nu = 0.97(3)$ [Eq. (10)], is larger than that of the magnetic susceptibility, $\gamma_{af}/\nu = -0.03(3)$ [Eq. (12)]. Therefore, the fidelity susceptibility $\chi_F^{(\theta)}$ admits a pronounced signature for the criticality as compared to the ordinary quantifiers such as the magnetic susceptibility. Such a feature is significant for the two-dimensional Ising antiferromagnet, where both specific heat and magnetic susceptibility exhibit weak (logarithmic) singularities at the Néel temperature. Last, we explain how the critical point $K_c|_{\theta=2.22} = 0.458\dots$ was extracted from Fig. 2 (d) of Ref. [29]. In Ref. [29], the partition-function zeros were calculated for the complex domain of $x = \exp(i\theta)$ with generic $\theta \in \mathbb{C}$; here, the reduced coupling constant K is fixed to $0.4 = \exp(-2K)$. In Fig. 2 (d) of Ref. [29], the accumulation of zeros forms a branch, which is about to touch the unit circle $x = \exp(i\theta)$ ($\theta \in \mathbb{R}$). Such a feature indicates that

the $\theta(\in \mathbb{R})$ -driven phase transition occurs at this crossing point. More specifically, we read off a couple of partition-function zeros $x_1 = -0.5014 + 0.4833i$ and $x_2 = -0.4644 + 0.3733i$, and found that the line defined by these points crosses the unit circle at $\theta = 2.22 \dots$. The above data are tabulated in Table 1. Nonetheless, we stress that the mechanism behind the phase transition differs from that of the ferromagnetic case [35], as noted in Ref. [29]. In the ferromagnetic case, the partition-function zeros simply forms a unit circle. Neither extra branch nor mutual crossing occurs, and no θ -driven phase transition takes place at all.

2.2 Scaling plot for $\chi_F^{(\theta)}$ with the fixed $\theta = 2.22$

In this section, in order to check the validity of the scaling analyses in Sec. 2.1, we present $\chi_F^{(\theta)}$'s scaling plot, which also sets a basis of the subsequent crossover-scaling analyses. The fidelity susceptibility obeys the scaling formula [15]

$$\chi_F^{(\theta)} = L^x f\left((K - K_c)L^{1/\nu}\right), \quad (13)$$

with $\chi_F^{(\theta)}$'s scaling dimension $x = \alpha_F^{(\theta)}/\nu$ and a non-universal scaling function f .

In Fig. 5, we present the scaling plot, $(K - K_c)L^{1/\nu} \chi_F^{(\theta)} L^{-\alpha_F^{(\theta)}/\nu}$, for various system sizes (+) $L = 16$, (\times) 18, and (*) 20 with the fixed $\theta = 2.22$. Here, we made a proposition $\nu = 1$ (two-dimensional-Ising universality), and the other scaling parameters are set to $K_c = 0.484$ [Eq. (8)], and $\alpha_F^{(\theta)}/\nu = 0.97$ [Eq. (10)]. The scaled data in Fig. 5 collapse into the scaling function f satisfactorily, validating the scaling analyses in Sec. 2.1 as well as the proposition $\nu = 1$. Hence, recollecting $\gamma_{af}/\nu = -0.03(3)$ [Eq. (12)], we confirm that the order-disorder phase transition indeed belongs to the two-dimensional-Ising universality class.

The scaling plot, Fig. 5, indicates that the fidelity susceptibility is less affected by the finite-size artifact [11]. Such a feature is favorable for the exact diagonalization method, with which the tractable system size is rather restricted. Encouraged by this observation, we proceed to examine how the order-disorder phase boundary terminates at the extremum point $\theta = \pi$.

2.3 Crossover-scaling plot for $\chi_F^{(\theta)}$ around $\theta \approx \pi$

In the above section, based on the scaling formula (13), we confirmed that the order-disorder-phase-transition branch belongs to the two-dimensional Ising universality class. In this section, by the agency of $\chi_F^{(\theta)}$, we further explore the end-point singularity of the phase boundary toward $\theta = \pi$. For that purpose, introducing yet another controllable parameter $\delta\theta = \pi - \theta$ and the accompanying crossover exponent ϕ , we consider the crossover-scaling formula [36,

37]

$$\chi_F^{(\theta)} = L^{\dot{x}} g \left((K - K_c(\theta)) L^{1/\dot{\nu}}, \delta\theta L^{\phi/\dot{\nu}} \right), \quad (14)$$

with the θ -dependent critical point $K_c(\theta)$, and a non-universal scaling function g . Here, the indices, \dot{x} and $\dot{\nu}$, are $\chi_F^{(\theta)}$'s scaling dimension and correlation-length critical exponent, respectively, right at $\delta\theta = 0$. As in Eq. (13), the index \dot{x} satisfies $\dot{x} = \dot{\alpha}_F^{(\theta)}/\dot{\nu}$ [15] with the fidelity-susceptibility critical exponent $\dot{\alpha}_F^{(\theta)}$ at $\delta\theta = 0$.

As explained in Sec. 1, the crossover exponent ϕ describes the shape of the phase boundary as $K_c \sim \delta\theta^{1/\phi}$ [36,37]. Hereafter, the crossover exponent ϕ is considered as an adjustable parameter, and the other indices, \dot{x} , $\dot{\alpha}_F^{(\theta)}$, and $\dot{\nu}$, are fixed in prior to the scaling analyses as follows. According to the duality theory [26], the hexagonal-lattice Ising antiferromagnet at $\theta = \pi$ reduces to the triangular-lattice antiferromagnet, and the uniform-susceptibility and correlation-length exponents are given by $\dot{\gamma}_{af} = 3/2$ and $\dot{\nu} = 1$, respectively [40]. Notably enough, through the duality, the frustrated (non-bipartite lattice) antiferromagnet comes out from the seemingly non-frustrated magnet, albeit with the imaginary magnetic field mediated. This is a peculiarity of the imaginary-field magnet, and such a character would not be captured properly by the mean-field treatment. These indices together with the relation $\dot{\alpha}_F^{(\theta)}/\dot{\nu} = \dot{\gamma}_{af}/\dot{\nu} + 1$ [15] (see Eq. (11)) immediately admit $\dot{x}(= \dot{\alpha}_F^{(\theta)}/\dot{\nu}) = 5/2$, which now completes the prerequisite for the crossover-scaling analysis.

In Fig. 6, we present the crossover-scaling plot, $(K - K_c(\theta))L^{-\chi_F^{(\theta)}}L^{-2.5}$, for various system sizes, (+) $L = 16$, (\times) 18, and (*) 20. Here, the second argument of the scaling function g is fixed to a constant value, $\delta\theta L^{\phi/\dot{\nu}} = 94.8$, with an optimal crossover exponent $\phi = 1.6$, and the critical point $K_c(\theta)$ was determined with the same scheme as that of Sec. 2.1. The crossover-scaled data in Fig. 6 collapse into a scaling curve; particularly, the data, (\times) $L = 18$ and (*) 20, are about to overlap each other, showing a tendency to the convergence as $L \rightarrow \infty$. Likewise, in Fig. 7 and 8, we present the crossover-scaling plot, $(K - K_c(\theta))L^{-\chi_F^{(\theta)}}L^{-2.5}$, with the crossover exponent, $\phi = 1.9$ and 1.3, respectively; the symbols are the same as those of Fig. 6. Here, the second argument of the scaling function g is set to $\delta\theta L^{\phi/\dot{\nu}} = 233$ and 38.6 in the respective analyses. In the former (latter) scaling plot, the left- (right-) side slope starts to split off, indicating that even larger (smaller) parameter ϕ leads a scatter of the scaled data. Hence, considering that these parameters set the tolerable bounds, we estimate the crossover exponent as

$$\phi = 1.6(3). \quad (15)$$

This is a good position to address a number of remarks. First, the underlying physics behind the crossover-scaling plot, Fig. 6, differs from that of the fixed- θ scaling plot, Fig. 5. Actually, the former scaling dimension $\dot{x} = 5/2$ is much larger than the latter $x = 1$, and hence, the data collapse of the crossover-scaling plot is by no means accidental. Second, the honeycomb-lattice Ising antiferromagnet enjoys the duality theory [26] so as to fix the critical indices such

as $\nu = 1$ and $\dot{\alpha}_F^{(\theta)}/\nu = 5/2$ [40]. Hence, it is anticipated that the crossover exponent $\phi = 1.6(3)$ [Eq. (15)] reflects the peculiarities of the honeycomb-lattice structure. Actually, the estimate $\phi = 1.6(3)$ [Eq. (15)] differs from the mean-field value $\phi = 1/2$ [34], whereas it is slightly suppressed as compared to the square-lattice case, $\phi = 2.0(4)$ [25]. Because the magnetic-susceptibility index for the honeycomb lattice $\dot{\gamma}_{af} = 3/2$ [40] is substantially smaller than that of the square lattice $5/2$ [41], it is reasonable that the multi-criticality depends on each lattice structure undertaken. Last, we mention a candidate for the quantifier other than the fidelity susceptibility. So far, the correlation length has played a significant role in the finite-size-scaling analyses. Actually, it is accessible via the diagonalization method [22], provided that the second-largest eigenvalue of the transfer matrix is at hand. The correlation length has an advantage in that it has a fixed scaling dimension $\sim L^1$ *a priori*. However, the second-largest eigenvalue is computationally demanding particularly for the non-hermitian transfer matrix, and this scheme was not accepted here.

3 Summary and discussions

The honeycomb-lattice Ising antiferromagnet (4) under the imaginary magnetic field $H = i\theta T/2$ was investigated with the transfer-matrix method [22]. As a probe to detect the phase transition, we utilized the extended version [17,24] of the fidelity (1), which makes sense even for such a non-symmetric complex-valued transfer matrix.

As a demonstration, we investigated the order-disorder phase transition for $\theta = 2.22$ with the fidelity susceptibility $\chi_F^{(\theta)}$ (6). Our result $K_c|_{\theta=2.22} = 0.484(4)$ [Eq. (8)] is comparable to that of the partition-function-zeros method, $K_c|_{\theta=2.22} = 0.458\dots$ [29], indicating that the probe $\chi_F^{(\theta)}$ detects the phase transition sensitively even in the presence of the imaginary magnetic field. Furthermore, we estimated $\chi_F^{(\theta)}$'s scaling dimension as $\alpha_F^{(\theta)}/\nu = 0.97(3)$ [Eq. (10)]. Through resorting to the scaling relation (11), we estimated magnetic-susceptibility's scaling dimension as $\gamma_{af}/\nu = -0.03(3)$ [Eq. (12)]. This result indicates that the criticality belongs to the two-dimensional-Ising universality class, $\gamma_{af} = 0$ (logarithmic) [38,39]. We then turn to the analysis of the end-point singularity of the phase boundary toward $\delta\theta (= \pi - \theta) \rightarrow 0$. With $\delta\theta$ scaled carefully, the $\chi_F^{(\theta)}$ data are cast into the crossover-scaling formula (14) [36,37]. Thereby, we estimated the crossover exponent as $\phi = 1.6(3)$ [Eq. (15)]. This result differs from the mean-field value $\phi = 1/2$ [34], whereas it is slightly suppressed as compared to that of the square-lattice model, $\phi = 2.0(4)$ [25]. It would be intriguing that the lattice structure renders subtle influences as to the end-point singularity. Actually, the honeycomb-lattice antiferromagnet at $\theta = \pi$ is under the reign of the duality theory [26,27,28,30], and it is anticipated that the end-point singularity reflect its peculiar characters.

According to Refs. [27,32,42], even in the ferromagnetic side $K < 0$, there should occur a singularity for generic values of $0 < \theta < \pi$; a notable point is that the transition is *not* the ordinary order-disorder phase transition [27].

Table 1 A comparison is made between the partition-function-zeros analysis [29] and ours. From an accumulation of zeros toward the unit circle $x = e^{i\theta}$ as shown in Fig. 2 (d) of Ref. [29], we read off the critical point $K_c = 0.458\dots (= -\ln 0.4/2)$ at $\theta = 2.22\dots$; see text for details. Our transfer-matrix method with the aid of the extended fidelity susceptibility (6) appears to support this elaborated pioneering study.

method	quantifier	$K_c _{\theta=2.22}$
partition-function zeros [29]	accumulation of zeros	0.458...
transfer matrix (present work)	fidelity susceptibility	0.484(4)

According to the partition-function-zeros survey [32], the transition point $|K_c|$ should locate around $\exp(-4|K_c|) \approx 0.8 (\neq 1)$ at $\theta = \pi/2$ as for the square lattice. Because the fidelity-susceptibility-mediated analysis does not require any *a priori* settings as to the order parameter, it would provide valuable information even for such an exotic singularity. This problem is left for the future study.

Acknowledgment

This work was supported by a Grant-in-Aid for Scientific Research (C) from Japan Society for the Promotion of Science (Grant No. 20K03767).

Author contribution statement

Y.N. conceived the presented idea, and performed the numerical simulations. He analyzed the numerical data, and wrote up the manuscript.

References

1. A. Uhlmann, Rep. Math. Phys. **9** (1976) 273.
2. R. Jozsa, J. Mod. Opt. **41** (1994) 2315.
3. A. Peres, Phys. Rev. A **30** (1984) 1610.
4. T. Gorin, T. Prosen, T. H. Seligman, and M. Žnidarič, Phys. Rep. **435** (2006) 33.
5. V. R. Vieira, J. Phys: Conference Series **213** (2010) 012005.
6. S.-J. Gu, Int. J. Mod. Phys. B **24** (2010) 4371.
7. A. Dutta, G. Aeppli, B. K. Chakrabarti, U. Divakaran, T. F. Rosenbaum and D. Sen, “Quantum Phase Transitions in Transverse Field Spin Models: From Statistical Physics to Quantum Information” (Cambridge University Press, Cambridge, 2015)
8. H. T. Quan, Z. Song, X. F. Liu, P. Zanardi, and C. P. Sun, Phys. Rev. Lett. **96** (2006) 140604.
9. P. Zanardi and N. Paunković, Phys. Rev. E **74** (2006) 031123.
10. H.-Q. Zhou, and J. P. Barjaktarevič, J. Phys. A: Math. Theor. **41** (2008) 412001.
11. W.-C. Yu, H.-M. Kwok, J. Cao, and S.-J. Gu, Phys. Rev. E **80** (2009) 021108.
12. W.-L. You and Y.-L. Dong, Phys. Rev. B **84** (2011) 174426.
13. V. Mukherjee, A. Polkovnikov, and A. Dutta, Phys. Rev. B **83** (2011) 075118.
14. D. Rossini and E. Vicari, Phys. Rev. E **98** (2018) 062137.
15. A. F. Albuquerque, F. Alet, C. Sire, and S. Capponi, Phys. Rev. B **81** (2010) 064418.
16. L. Wang, Y.-H. Liu, J. Imriška, P. N. Ma, and M. Troyer, Phys. Rev. X **5** (2015) 031007.
17. D. Schwandt, F. Alet, and S. Capponi, Phys. Rev. Lett. **103** (2009) 170501.
18. C. De Grandi, A. Polkovnikov, and A. W. Sandvik, Phys. Rev. B **84** (2011) 224303.
19. J. Zhang, X. Peng, N. Rajendran, and D. Suter, Phys. Rev. Lett. **100** (2008) 100501.

Fig. 1 (a) A schematic θ - K phase diagram is presented for the honeycomb-lattice Ising antiferromagnet (4) under the imaginary magnetic field $H = i\theta T/2$; here, the reduced coupling constant K is given by $K = J/T$. The overall feature should resemble the square-lattice case [32, 33]; a notable point is that unlike the ferromagnetic counterpart [35], the order-disorder phase boundary extends into the $\theta > 0$ regime. The phase boundary ends up at $\theta = \pi$, where a number of rigorous results are available [26, 27, 28]. (b) The end-point behavior of the phase boundary around $\theta \approx \pi$ may depend on the lattice structure undertaken. The mean-field analysis [34] suggests that the phase boundary exhibits a convex curvature characterized [36, 37] by the small crossover exponent $\phi = 1/2 (< 1)$. On the one hand, For the square-lattice model, a concave curvature $\phi > 1$ was suggested via the partition-function-zeros [32] and series-expansion [33] analyses; see Ref. [25] as well. Then, there arises a problem how the honeycomb-lattice structure influences the crossover exponent ϕ .

20. M. Kolodrubetz, V. Gritsev, and A. Polkovnikov, Phys. Rev. B **88** (2013) 064304.
21. S.-J. Gu and W. C. Yu, Europhys. Lett. **108** (2014) 20002.
22. P. de Forcrand and T. Rindlisbacher, EPJ web of conferences **175** (2018) 07026.
23. H.-Q. Zhou, R. Orús, and G. Vidal, Phys. Rev. Lett. **100** (2008) 080601.
24. J. Sirker, Phys. Rev. Lett. **105** (2019) 117203.
25. Y. Nishiyama, arXiv:2005.10373.
26. H. Imaoka and Y. Kasai, J. Phys. Soc. Japan **65** (1996) 725.
27. M. Suzuki, J. Phys. Soc. Japan **60** (1990) 441.
28. K. Y. Lin and F. Y. Wu, Int. J. Mod. Phys. B **2** (1988) 471.
29. S.-Y. Kim, Phys. Rev. E **82** (2010) 041107.
30. V. Matveev and R. Shrock, J. Phys. A: Math. Theor. **29** (1996) 803.
31. V. Matveev and R. Shrock, Phys. Rev. E **53** (1996) 254.
32. V. Matveev and R. Shrock, J. Phys. A: Math. Theor. **41** (2008) 135002.
33. V. Azcoiti, G. Di Carlo, E. Follana, and E. Royo-Amondarain, Phys. Rev. E **96** (2017) 032114.
34. V. Azcoiti, E. Follana, and A. Vaquero, Nucl. Phys. B **851** (2011) 420.
35. T. D. Lee and C. N. Yang, Phys. Rev. **87** (1952) 410.
36. E.K. Riedel and F. Wegner, Z. Phys. **225** (1969) 195.
37. P. Pfeuty, D. Jasnow, and M. E. Fisher, Phys. Rev. B **10** (1974) 2088.
38. M.E. Fisher, Proc. R. Soc. London A **254** (1960) 66.

Fig. 2 A unit of the transfer-matrix slice for the honeycomb-lattice Ising antiferromagnet (4) is shown. The row-to-row statistical weight between the spin configurations, $S_{1,2,\dots,L}$ and $T_{1,2,\dots,L}$, yields the transfer matrix element $T_{\{S_i\},\{T_i\}}$. The transfer matrix T is not symmetric as would be apparent from the drawing. The periodic-boundary condition such as $S_{L+1} = S_1$ and $T_{L+1} = T_1$ is imposed.

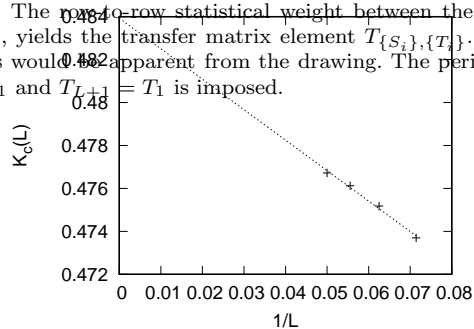


Fig. 3 The approximate critical point $K_c(L)$ (7) is plotted for $1/L$ with the fixed imaginary magnetic field $\theta = 2.22$. The least-squares fit to the data yields an estimate $K_c = 0.48392(55)$ in the thermodynamic limit $L \rightarrow \infty$. A possible systematic error is considered in the text.

39. M. Kaufman, Phys. Rev. B **36** (1987) 3697.
40. T. Horiguchi, K. Tanaka, and T. Morita, J. Phys. Soc. Japan **61** (1992) 64.
41. V. Matveev and R. Shrock, J. Phys. A: Math. Theor. **28** (1995) 4859.
42. P. Sarkanych, Y. Holovatch, and R. Kenna, J. Phys. A: Math. Theor. **51** (2018) 505001.

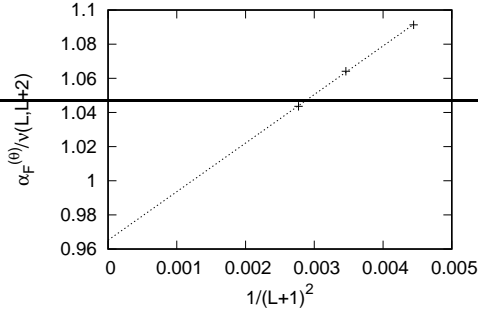


Fig. 4 The approximate critical exponent $\alpha_F^{(\theta)}/\nu(L, L+2)$ (9) is plotted for $1/(L+1)^2$ with the fixed imaginary magnetic field $\theta = 2.22$. The least-squares fit to the data yields an estimate $\alpha_F^{(\theta)}/\nu = 0.0062(22)$ in the thermodynamic limit $L \rightarrow \infty$. A possible systematic error is considered in the text.

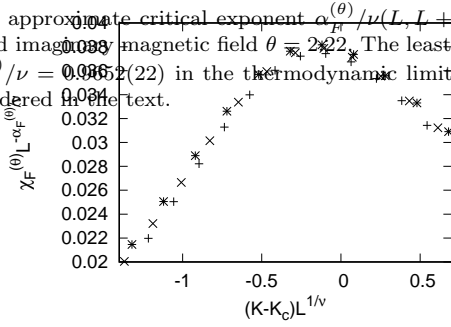


Fig. 5 The scaling plot, $(K - K_c)L^{1/\nu} - \chi_F^{(\theta)} L^{-\alpha_F^{(\theta)}/\nu}$, is presented with $K_c = 0.484$ [Eq. (8)], $\alpha_F^{(\theta)}/\nu = 0.97$ [Eq. (10)], and $\nu = 1$ (2D-Ising universality) for various system sizes, (+) $L = 16$, (x) 18, and (*) 20; see the scaling formula (13). The scaled data seem to fall into the scaling curve satisfactorily, validating the scaling analyses in Sec. 2.1 and the proposition $\nu = 1$.

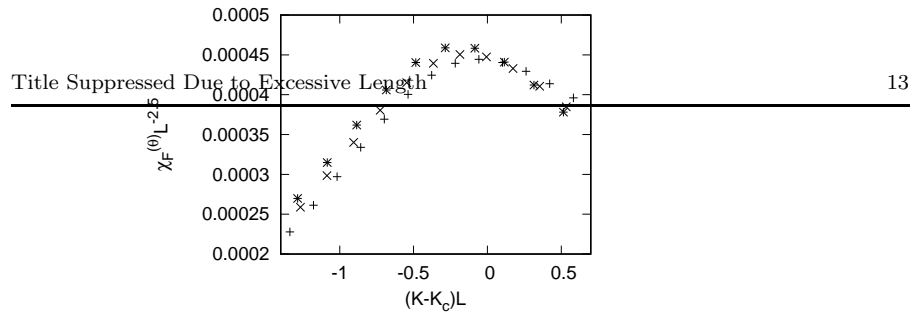


Fig. 6 The crossover-scaling plot, $(K - K_c(\theta))L - \chi_F^{(\theta)} L^{-2.5}$, is presented with the second argument of the scaling function g fixed to $\delta\theta L^\phi = 94.8$ and the crossover exponent $\phi = 1.6$ for various system sizes $L = 16$, (\times) 18, and $(*)$ 20; see the crossover-scaling formula (14). The crossover-scaled data fall into a scaling curve. Particularly, the data, (\times) $L = 18$ and $(*)$ 20, are about to overlap each other, suggesting that the proposition $\phi = 1.6$ is an optimal one.

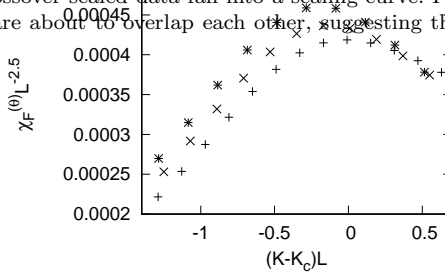


Fig. 7 The crossover-scaling plot, $(K - K_c(\theta))L - \chi_F^{(\theta)} L^{-2.5}$, is presented with the second argument of the scaling function g fixed to $\delta\theta L^\phi = 233$ and the crossover exponent $\phi = 1.9$; see the crossover-scaling formula (14). The symbols, $(+)$, (\times) , and $(*)$, are the same as those of Fig. 6. The left-side slope gets resolved as for large ϕ .

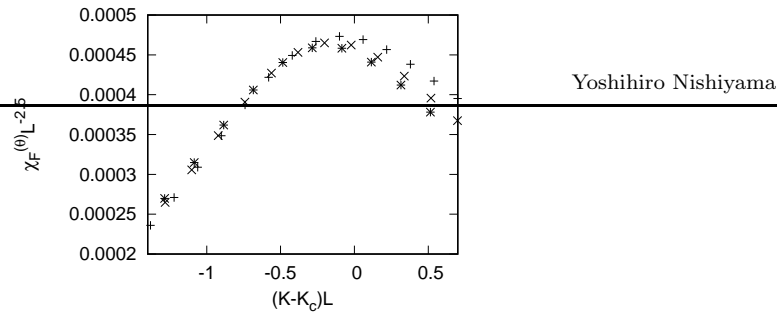


Fig. 8 The crossover-scaling plot, $(K - K_c(\theta))L - \chi_F^{(\theta)} L^{-2.5}$, is presented with the second argument of the scaling function g fixed to $\delta\theta L^\phi = 38.6$ and the crossover exponent $\phi = 1.3$; see the crossover-scaling formula (14). The symbols, (+), (\times), and (*), are the same as those of Fig. 6. The right-side slope splits off as for small ϕ .